Microstructured Optical Fibers : from linear to nonlinear modelling

Survey of the numerical methods developed at the Institut Fresnel

Gilles Renversez, Université d'Aix-Marseille, Institut Fresnel CNRS

Institut Fresnel (UMR CNRS 6133) & Université d'Aix-Marseille
gilles.renversez@fresnel.fr

Jornadas Valencianas de Fotónica Computacional
Intertech, Universidad Polytécnica de Valencia, 28/10/2010

Introduction I
Definition

- A **microstructured optical fiber** (MOF) is a fiber composed of a set of inclusions with various shapes or refractive indices embedded in a glass matrix.
- These inclusions confine the electromagnetic field.

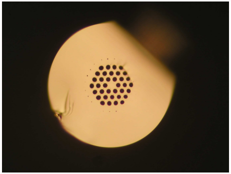

made of chalcogenide glass (LVC, Université de Rennes/Perfos)

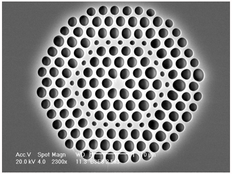

made of silica (X-lim, Université de Limoges)

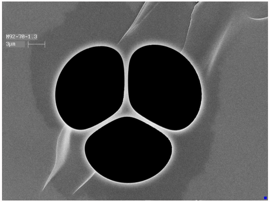

suspended core MOF made of As_2S3, core size $\approx 2.3\ \mu$m (ICB, Université de Bourgogne)

Figure: Examples of solid core MOFs

Introduction II
Definition

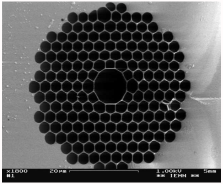

silica one (Phlam / IRCICA, Université de Lille I)

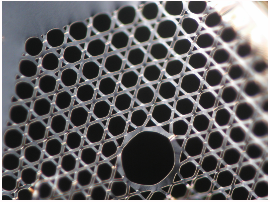

chalcogenide $Te_2As_3Se_5$, (Univ. de Rennes, PERFOS). $\varnothing_{coeur} \simeq 28.9\mu$m. $\lambda_{BIP} \simeq 9.3\ \mu$m, $n_{mat} \simeq 2.93$

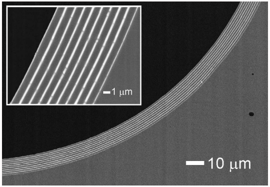

Bragg fiber made of polymer and chalcogenide (MIT/Harvard University)

Figure: Examples of hollow core MOFs

MOFs have at least two advantages compared to conventional fibers:

- The geometrical parameter space is much wider
- The refractive index contrasts vary from less than 1% to 200%

Introduction
Brief historical note

- Suspended core MOFs have been built since 1973 : **Kaiser, Marcatili and Miller published the first experimental and theoretical study on MOFs :** *A New Optical Fiber* in *Bell Syst. Tech. J., vol. 52, p. 265-269*, 1973.

THE BELL SYSTEM TECHNICAL JOURNAL, FEBRUARY 1973

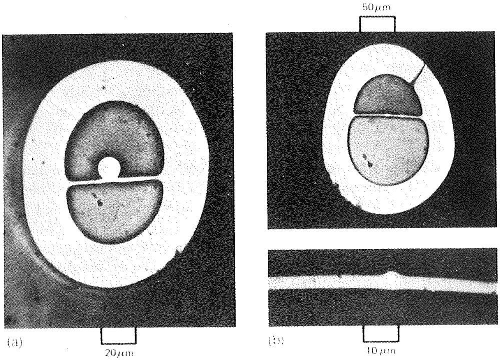

FIG. 2—Photographs of an experimental (a) multimode SM fiber and (b) single-mode SM fiber (top), with magnified core region (bottom).

MOFs made of Suprasil 2 :
(a) $\mathcal{L}_{dB} \simeq$ 28 dB/km at 1.06 μm.
(b) $\mathcal{L}_{dB} \simeq$ 55 dB/km at 1.06 μm.

A complementary article written by Kaiser and Astle was published in 1974 in the same journal.

Guiding in microstructured or not fibers
Guiding in conventional fibers

- Invariance by translation can be assumed : $\lambda \sim 1\mu$m et $L \gtrsim 1$m.
- We seek for solutions for the electromagnetic fields in the form: $\mathbf{V}(r, \theta) \exp(-i(\omega t - \beta z))$.
- We solve Maxwell equations.
- We solve the homogeneous problem (no incident field) to get the **modes**.

The propagation constant β is the key parameter of modes.
effective index $n_{eff} \equiv \beta / k_0$

Guiding in microstructured or not fibers

Dispersion for a step-index fiber

Without any material losses *i.e.* $\Im m(n_{mat}) = 0$

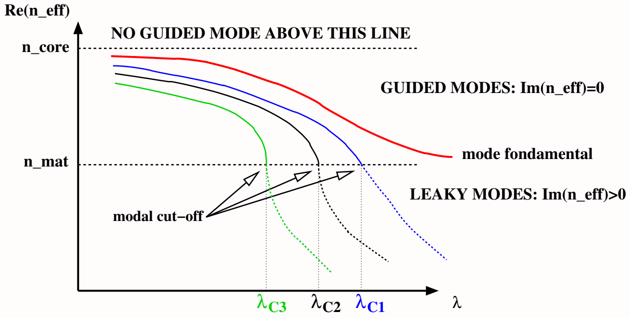

Figure: Scheme of the dispersion curves $\Re e(n_{eff})$ of the first modes

- Modes exist after the cutoff wavelength λ_C: they become leaky modes
- Guiding losses are directly linked to $\Im m(n_{eff}) = \Im m(\beta/k_0)$

Guiding in microstructured or not fibers

For a solid core MOF with low index inclusions

- Modes are not prefectly guided, even if $\Im m(n_{mat}) = 0$, they are leaky modes: $\Im m(n_{eff}) > 0$

-Λ est the lattice pitch
-d is the inclusion diameter
-N_r is the number of rings

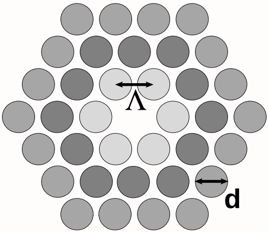

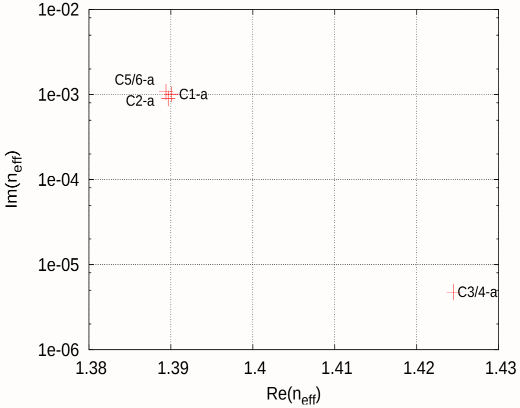

Complex effective indices of the "first" modes

Numerical methods to study MOFs
Common features of the detailed vector methods

1. We seek solutions for modes, in the form: $\mathbf{V}(r,\theta)\exp(-i(\omega t - \beta z))$.
2. We solve rigorously Maxwell equations.
3. We set the problem as a scattering problem $\longrightarrow$ homogeneous problem to get the modes.
4. $\beta \in \mathbb{C}$ ou $\in \mathbb{R}$, β and the fields are the unknown. (direct formulation : $\beta(\omega)$ and not $\omega(\beta)$).
5. We model finite size and periodic structures.
6. We take into account spatial symmetry properties of tranverse MOF profile.
7. No *a priori* information is required about the fields.
8. Material dispersions can be take into account.

Numerical methods to study MOFs

The multipole method (1)

Few equations

- In the glass matrix, fields fulfill Helmholtz equation.
- We know how to express the transverse components as a function of the two longitudinal components
- We develop these components E_z et H_z in Fourier-Bessel series around each inclusion:

$$\left\{ \begin{array}{lcl} E_z(r,\theta,z) & = & \sum_{n\in\mathbb{Z}}[A_n^E J_n(k_\perp r) + B_n^E H_n^{(1)}(k_\perp r)]e^{in\theta}e^{i\beta z} \\ H_z(r,\theta,z) & = & \sum_{n\in\mathbb{Z}}[A_n^H J_n(k_\perp r) + B_n^H H_n^{(1)}(k_\perp r)]e^{in\theta}e^{i\beta z} \end{array} \right.$$

- We build vectors $\mathbf{A_l}$ et $\mathbf{B_l}$ with coef. A_n et B_n of l'inclusion l

Numerical methods to study MOFs
The multipole method (2)

Scattering matrices of one inclusion $\mathbf{S_l}$

- $\mathbf{A_l} \simeq$ incident field and $\mathbf{B_l} \simeq$ scattered field by inclusion l
- $\mathbf{B_l} = \mathbf{S_l}\mathbf{A_l}$
- If inclusion is circular then $\mathbf{S_l}$ is known analytically as a function of J_n et $H_n^{(1)}$

Field consistency, Rayleigh identity

- Matrix to change the basis $\mathcal{H}_{j,l}$ (Graf addition theorem)
- Incident field in inclusion l = scattered field by all the others + direct incident field:

$$\mathbf{A_l} = \sum_{j \neq l} \mathcal{H}_{j,l}\mathbf{B_j} + \mathcal{H}_{0,l}\mathbf{B_0}$$

Numerical methods to study MOFs
The multipole method (3)

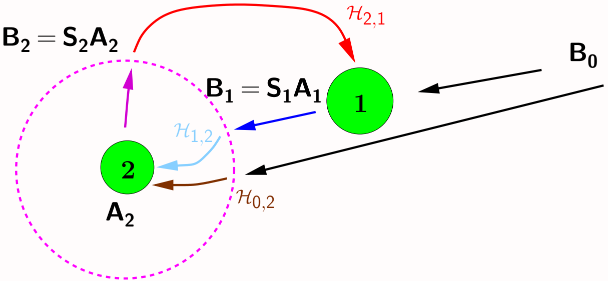

Figure: Scheme of principle of the multipole method: self-consitency of the indicent and scattered fields by the sed of inclusions

Matrix equation of the method

$$\left\{ \begin{array}{l} \mathbf{B_1} = \mathbf{S_1}(\sum_{j\neq 1}\mathcal{H}_{j,1}\mathbf{B_j} + \mathcal{H}_{0,1}\mathbf{B_0}) \\ \mathbf{B_2} = \mathbf{S_2}(\sum_{j\neq 2}\mathcal{H}_{j,2}\mathbf{B_j} + \mathcal{H}_{0,2}\mathbf{B_0}) \\ \dots \end{array} \right. \qquad \text{soit} \qquad \mathcal{M}\begin{bmatrix} \mathbf{B_1} \\ \mathbf{B_2} \\ \dots \end{bmatrix} = \mathcal{D}\begin{bmatrix} \mathbf{B_0} \\ \mathbf{B_0} \\ \dots \end{bmatrix}$$

Numerical methods to study MOFs
The multipole method (4)

$\mathcal{M}$ matrix and the modes

- $\mathcal{M}$ depends on λ, β, and on the inclusion parameters
- A mode corresponds to a propagating field without external sources ($\mathbf{B_0} = 0$):

$$\mathcal{M} \begin{bmatrix} \mathbf{B_1} \\ \mathbf{B_2} \\ \dots \end{bmatrix} = 0 \text{ avec } \mathbf{B_l} \text{ non nuls}$$

$$det\mathcal{M}(\beta) = 0 \text{ (équation de dispersion d'une FOM)}$$

- β being determined, we compute the fields through the eigen vectors of $\mathcal{M}$

Practical but crucial issue

Mode problems are harder to solve numerically that scattering problems. The efficient search of the β in $\mathbb{C}$ such that $det\left(\mathcal{M}(\beta)\right) = 0$ is not trivial . . .

Numerical methods to study MOFs

Differential method with FFF

Principles

1. differential method in cylindrical coordinates (r, θ, z) and in conical mounting
2. use of the correct factorization rules for Fourier series
3. use of the S algorithm
4. scattering problem $\longrightarrow$ mode problem

Split the space in 3 regions

- 2 homogeneous regions
  explicit expression for the fields
- 1 intermediate region: modulated zone
  differential system of 1^{er} order ein r to be solved numerically

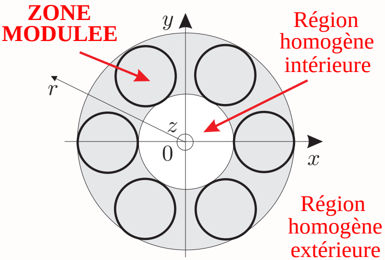

After the computations of the $S^{(i)}$ matrices across the modulated zone

Scattering matrix S of the modulated zone: $\mathbf{S}^{-1}\mathbf{B} = \mathbf{A}$

Numerical methods to study MOFs
Finite element method (1)

Principles

1. spatial discretization: mesh and basis function
   $\psi(x, y) \quad \rightsquigarrow \quad \sum_{j=1}^{\text{nb él.}} \psi_j \alpha_j(x, y)$
2. weak formulation of Maxwell equations : integral formulation
3. numerical resolution involving only sparse matrices

Numerical methods to study MOFs
Finite element method (2)

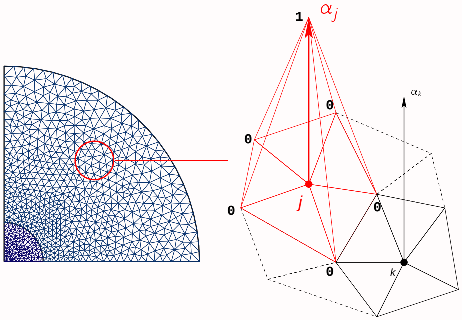

Figure: Mesh on a quater of the fiber cross section and form functions in the scalar case

Numerical methods to study MOFs I
Finite element method (3)

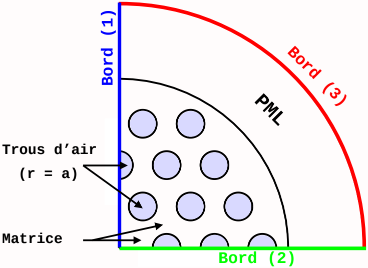

Geometry

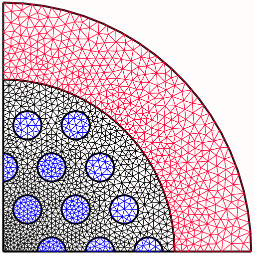

Mesh

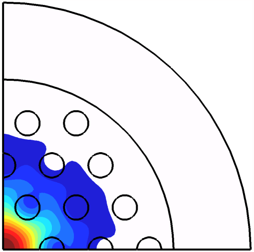

$|S_z|$ for the fundamental mode

Figure: for a solid core MOF

Technical difficulty

- Definition and use of 'Perfect Matching Layer' (PML)

Numerical methods to study MOFs

Finite element method: vector case (4)

Vector equation

directly from Maxwell equations:

$$\nabla \times (\nabla \times \mathbf{E}) = k_0^2 \epsilon_r(x, y)$$

Type of the solutions

$$\mathbf{E} = \left(\mathbf{E_t} + E_z \mathbf{e_z}\right) e^{i\beta z - i\omega t}$$

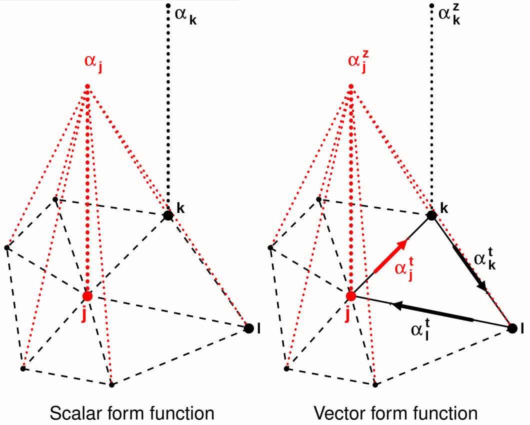

Numerical methods to study MOFs

Symmetries of the MOFs and of their modes

Symmetrie of the section: examples of C_n ou C_{nv} types

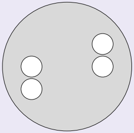

C_2 (no symmetry plane)

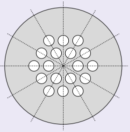

C_{6v} (6 symmetry planes)

Figure: The section is invariant by $2\pi/n$ rotations.

Numerical methods to study MOFs

Symmetries of the MOFs and of their modes

Symmetrie of the section: examples of C_n ou C_{nv} types

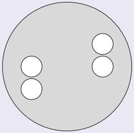

C_2 (no symmetry plane)

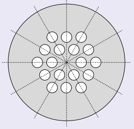

C_{6v} (6 symmetry planes)

Figure: The section is invariant by $2\pi/n$ rotations.

Symmetries of the modes and degeneracies for the C_{6v} cases : 8 classes et 2 irreducible geometric sectors (McIsaac 1975)

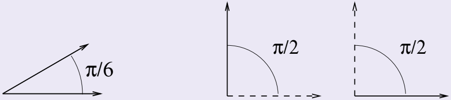

p=2 **p=3 and p=4**

Figure: 3 among the 8 symmetry classes with the corresponding irreducible geometric sectors

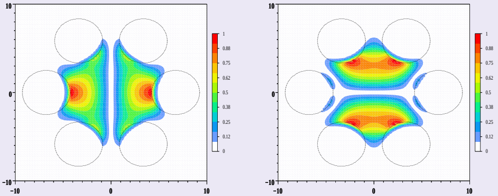

$|E_z|$ for $p = 3$ $|E_z|$ for $p = 4$

Numerical methods to study MOFs
Comparison between the 3 numerical methods

- consider finite size structures
- get the losses
- take into account symmetries
- take into account material dispersion

All these 3 methods have been developped and implemented at the lab.

- The MM and the FEM are well suited to be adapted to study periodic structures : compute band diagrams

Numerical methods to study MOFs
Comparison between the 3 numerical methods

Méthode Multipolaire (MM)

Temps de calcul:

Le plus faible

Précision:

La meilleure sur $\Re e(n_{eff})$

et sur $\Im m(n_{eff})$

Avantages:

1. Calculs semi-analytiques pour des inclusions circulaires
2. Nombre de couches d'inclusions élevé

Limitations:

1. Milieux homogènes et isotropes
2. Les inclusions inscrites dans des cercles non-sécants
3. Pour inclusion non-circulaire:

Méthode différentielle (MD)

Temps de calcul:

$>$ MM

Précision:

$>$ MEF mais $<$ MM

Avantages:

1. Géométrie arbitraire
2. Milieux inhomogènes et anisotropes
3. Mise en place des symétries

Limitations:

1. Nombre de couches d'inclusions
2. Intégration numérique
3. Codage des structures

Méthode des éléments finis avec gmsh/getdp (MEF)

Temps de calcul:

$>$ MM, $\lesssim$ MD

Précision:

$<$ MM, $\lesssim$ MD pour $\Im m(n_{eff})$

Avantages:

1. Géométrie arbitraire
2. Milieux inhomogènes et anisotropes
3. Codage des structures

Limitations:

1. Modes à pertes $\Rightarrow$ PML
2. Plusieurs paramètres internes
3. Nombre de couches d'inclusions

Numerical methods to study MOFs
Computing band diagram using the finite element method (1)

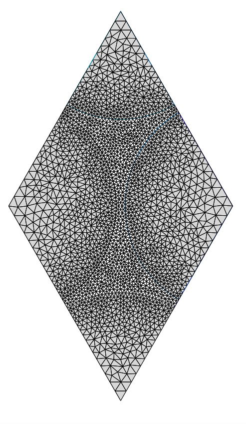

Meshing of a basic rhombic cell with 4628 triangles.

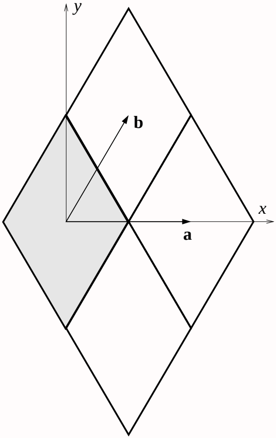

Representation of some lattice cells with the lattice vectors $\mathbf{a} = \Lambda \mathbf{e}_x$ and $\mathbf{b} = \frac{\Lambda}{2}\mathbf{e}_x + \frac{\Lambda\sqrt{3}}{2}\mathbf{e}_y$.

Numerical methods to study MOFs
Computing band diagram using the finite element method (2)

Two-dimensional periodic structure: the triangular lattice of circular inclusions. The basic cell is rhombic with a side length Λ with a circular air inclusion with a radius $R = 0.48\Lambda$.

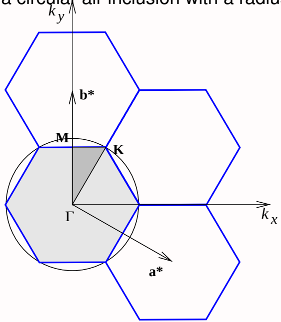

Some cells of the reciprocal lattice with the lattice vectors

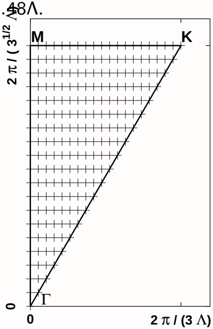

Example of sampling points in the irreducible part of the Brillouin zone (IBZ) for a triangular lattice. 210 points are used in this case to sample in 2D the IBZ.

Nonlinear properties of suspended core MOFs

Toward supercontinuum in the mid-infrared

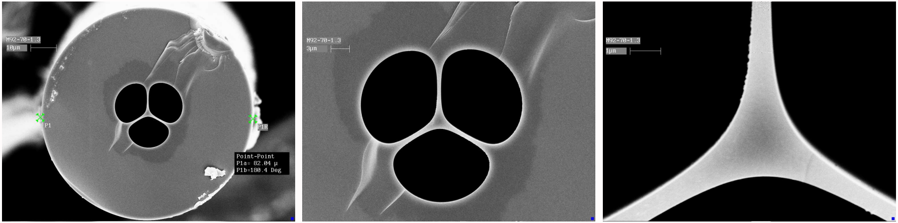

core size $\approx 2.3\ \mu m$

Figure: First As_2S_3 and As_2Se_3 suspended core MOFs : LVC ,Université de Rennes I, and ICB, Université de Bourgogne

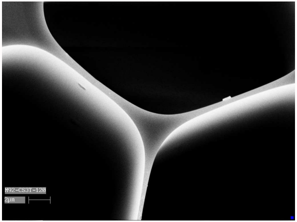

Nonlinear properties of suspended core MOFs
Comparisons experiments/simulations with the GNLSE

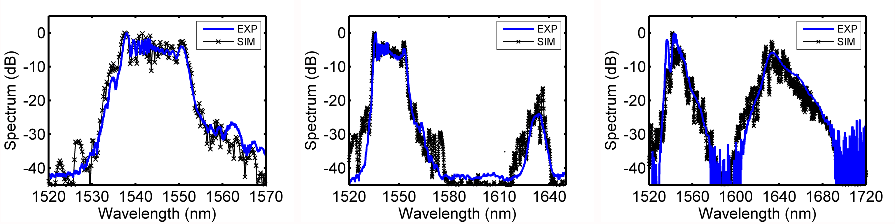

18 W 28 W 54 W

Figure: Output spectra recorded from 1.8m long 2.6 μm core As_2S_3 MOF for 3 input powers

- The agreement between the experiments and the simulations is fairly good.
- The computed curves are obtained with $\gamma = 2150\text{W}^{-1}.\text{km}^{-1}$.
- Spontaneaous Raman scattering Stockes wave at 1.635 μm with a 85 nm shift

Conclusion

- The **wide optogeometric parameter space** available in MOFs allow a tight control of their linear properties.
- These linear properties allow to manage efficiently nonlinear properties.

More complex structures can be achieved from MOFs:

- tapers: to enhanced or to tune nonlinear effects to to use evanescent fields
- fibers with metallic inclusions

To use at their best these fibers, one must understand their physical properties and one must be able to model them precisely.

MOF linear properties

Dropped work : Spatial solitons

Spatial solitons in waveguides with a Kerr nonlinearity: Beyond the Townes soliton

Numerical method:

- Our algorithm to find self-coherent nonlinear solutions (spatial solitons) is convergent, and accurate.
- We are able to compute these self coherent nonlinear solutions of the scalar and full Maxwell's problems.

Physical results:

- We generalize the Townes soliton taking into account:
  - the propagation constant
  - the optogeometric cross section of the waveguide
- Our nonlinear solutions in finite size waveguides:
  - converge towards the Townes soliton in the short wavelength limit but differ in other cases
  - have an higher power than the Townes soliton for long wavelengths

Spatial solitons: beyond Townes soliton

Some personal references I
inverse chronological order

M. El-Amraoui, J. Fatome, J. C. Jules, B. Kibler, G. Gadret, C. Fortier, F. Smektala, I. Skripatchev, C.F. Polacchini, Y. Messaddeq, J. Troles, L. Brilland, M. Szpulak, and G. Renversez.
Strong infrared spectral broadening in low-loss As-S chalcogenide suspended core microstructured optical fibers.
Opt. Express, 18(5):4547–4556, 2010.

F. Désévédavy, G. Renversez, J. Troles, P. Houizot, L. Brilland, I. Vasilief, Q. Coulombier, N. Traynor, F. Smektala, and J.-L. Adam.
Chalcogenide glass hollow core photonic crystal fibers.
Optical Materials, 32:1532–1539, 2010.

Q. Coulombier, L. Brilland, P. Houizot, Thierry Chartier, T.-N. N'Guyen, F. Smektala, G. Renversez, A. Monteville, D. Méchin, T. Pain, H. Orain, J.-C. Sangleboeuf, and Johann Trolès.
Casting method for low-loss chalcogenide microstructured optical fibers.
Opt. Express, 18(9):9107–9112, 2010.

F. Désévédavy, G. Renversez, J. Troles, L. Brilland, P. Houizot, Q. Coulombier, F. Smektala, N. Traynor, and J.-L. Adam.
Te-As-Se glass microstructured optical fiber for the middle infrared.
Appl. Opt., 48(19):3860–3865, 2009.

F. Drouart, G. Renversez, A. Nicolet, and C. Geuzaine.
Spatial Kerr solitons in optical fibres of finite size cross section: beyond the Townes soliton.
J. Opt. A: Pure Appl. Opt., 10:125101, 2008.

Some personal references II
inverse chronological order

L. Brilland, J. Troles, P. Houizot, F. Désévédavy, Q. Coulombier, G. Renversez, T. Chartier, T.N. Nguyen, J.L. Adam, and N. Traynor.
Interface impact on the transmission of chalcogenide photonic crystal fibres.
Journal of the Ceramic Society of Japan, 116, 2008.

F. Désévédavy, G. Renversez, L. Brilland, P. Houizot, J. Troles, Q. Coulombier, F. Smektala, N. Traynor, and J.-L. Adam.
Small-core chalcogenide microstructured fibers for the infrared.
Appl. Opt., 47(32):6014–6021, 2008.

P. Boyer, G. Renversez, E. Popov, and M. Nevière.
Improved differential method for microstructured optical fibres.
J. Opt. A: Pure Appl. Opt., 9:728–740, 2007.

G. Renversez, P. Boyer, and A. Sagrini.
Antiresonant reflecting optical waveguide microstructured fibers revisited: a new analysis based on leaky mode coupling.
Opt. Express, 14(12), 2006.

L. Brilland, F. Smektala, G. Renversez, T. Chartier, J. Troles, T. Nguyen, N. Traynor, and A. Monteville.
Fabrication of complex structures of holey fibers in chalcogenide glass.
Opt. Express, 14(3):1280–1285, 2006.

Some personal references III
inverse chronological order

- L. Labonté, D. Pagnoux, P. Roy, F. Bahloul, M. Zghal, G. Mélin, E. Burov, and G. Renversez.
  Accurate measurement of the cutoff wavelength in a microstructured optical fiber by means of an azimuthal filtering technique.
  Opt. Lett., 31:1779–1781, 2006.
- P. Boyer, G. Renversez, E. Popov, and M. Nevière.
  A new differential method applied to the study of arbitrary cross section microstructured optical fibers.
  Opt. and Quant. Electron., 38:217–230, 2006.
- F. Zolla, G. Renversez, A. Nicolet, B. Kuhlmey, S. Guenneau, and D. Felbacq.
  Foundations of Photonic Crystal Fibres.
  Imperial College Press, London, 2005.
- G. Renversez, F. Bordas, and B. T. Kuhlmey.
  Second mode transition in microstructured optical fibers: determination of the critical geometrical parameter and study of the matrix refractive index and effects of cladding size.
  Opt. Lett., 30(11):1264–1266, 2005.
- G. Renversez, B. Kuhlmey, and R. McPhedran.
  Dispersion management with microstructured optical fibers: Ultra-flattened chromatic dispersion with low losses.
  Opt. Lett., 28(12):989–991, 2003.

Some personal references IV
inverse chronological order

B. Kuhlmey, T. P. White, G. Renversez, D. Maystre, L.C. Botten, C. M. de Sterke, and R. C. McPhedran.
Multipole method for microstructured optical fibers II: implementation and results.
J. Opt. Soc. Am. B, 10(19):2331–2340, 2002.

Justification du modèle avec matrice infinie pour la FOM

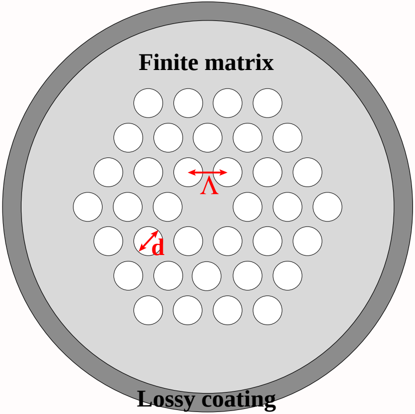

configuration expérimentale

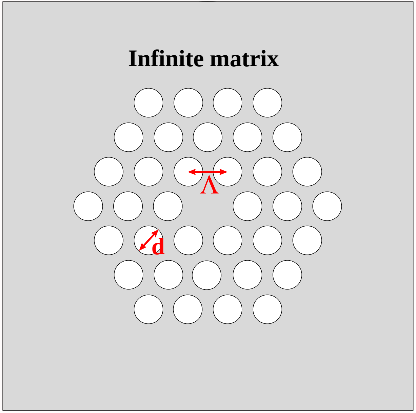

configuration employée pour la modélisation

Des méthodes numériques pour étudier les FOM
La méthode différentielle (1) (Boyer, Popov, Nevière)

Principles

1. méthode différentielle en coordonnées cylindriques (r, θ, z)
2. utilisation des règles correctes de factorisation
3. utilisation de l'algorithme S

Partage de l'espace en trois régions

- 2 régions homogènes
  expressions explicites des champs
- 1 région intermédiaire: la zone modulée
  système différentiel à intégrer numériquement

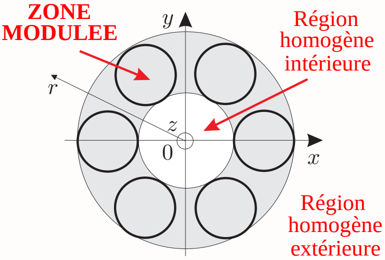

Des méthodes numériques pour étudier les FOM
La méthode différentielle (2)

Dans la zone modulée:

- $\mathbf{D}(r,\theta,z) = \epsilon(r,\theta)\mathbf{E}(r,\theta,z)$
- développements de Fourier de $\begin{cases} \mathbf{D}(r,\theta,z) \\ \mathbf{E}(r,\theta,z) \end{cases}$
- développement de Fourier de $\epsilon(r,\theta)$

Règles de factorisation (L. Li (1996))

- **Règle directe:** $[\mathbf{D}_T] = [\![\epsilon]\!]\,[\mathbf{E}_T]$
- **Règle inverse:** $[\mathbf{D}_N] = \left[\!\!\left[\frac{1}{\epsilon}\right]\!\!\right]^{-1} [\mathbf{E}_N]$
- Expression de $[\mathbf{E}_T]$ et $[\mathbf{E}_N]$ en fonction de $[\mathbf{E}]$

$\Rightarrow$ $[\mathbf{D}] = Q_\epsilon\,[\mathbf{E}]$ (la matrice Q_ϵ n'est pas simple)

Notation: $[\![\epsilon]\!] = \begin{pmatrix} & \vdots & \\ & \epsilon_{n-m} & \dots \\ & & \end{pmatrix}$

Des méthodes numériques pour étudier les FOM
La méthode différentielle (3)

Intégration numérique à travers la zone modulée

Matrice de transmission T de la zone modulée

$$\mathbf{U} = \mathbf{TV} \quad \text{avec} \left\{ \begin{array}{l} \text{U: Coef. de Fourier des champs} \\ \text{dans la région homogène extérieure} \\ \text{V: Coef. de Fourier des champs} \\ \text{dans la région homogène intérieure} \end{array} \right.$$

Si e trop grand

1. Divergence de certains éléments de la matrice T
2. Contaminations numériques

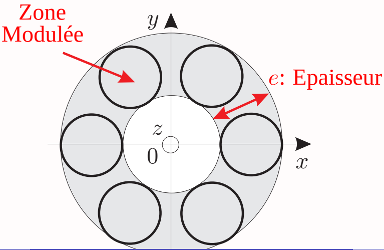

Des méthodes numériques pour étudier les FOM
La méthode différentielle (4)

Principe de l'algorithme S

- Subdivision de la zone modulée en sous-zones modulées
- Pour la sous-zone modulée $n^o\ i$:
  1. **Intégration**:
     Arrêt avant contaminations numériques
     $\Rightarrow$ matrice $T^{(i)}$ bien conditionnée
  2. **Calcul itératif:** $S^{(i)} = f\left(S^{(i-1)}, T^{(i)}\right)$
     dont les éléments sont bornés

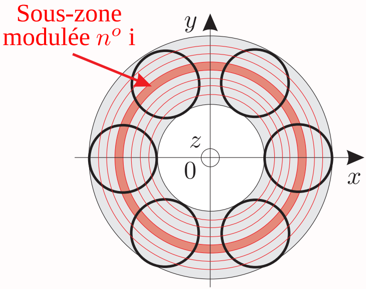

Après calcul des matrices $S^{(i)}$ à travers la zone modulée

Matrice de diffraction S de la zone modulée:

$$\mathbf{B} = \mathbf{S}\mathbf{A} \quad \text{avec} \begin{cases} \text{B: Coefficient de Fourier des champs diffractés} \\ \text{A: Coefficient de Fourier des champs incidents} \end{cases}$$

Des méthodes numériques pour étudier les FOM
La méthode de type élements finis: cas vectoriel (2)

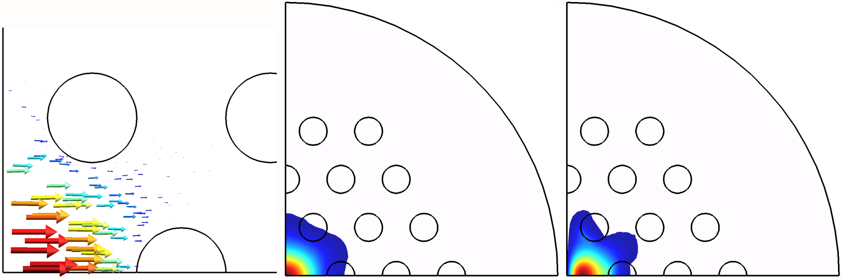

$\mathbf{E_t}$ $|\mathbf{E_t}|$ E_z

Interprétation en termes de diagramme de bandes

FOM à cœur solide avec des inclusions de bas indice

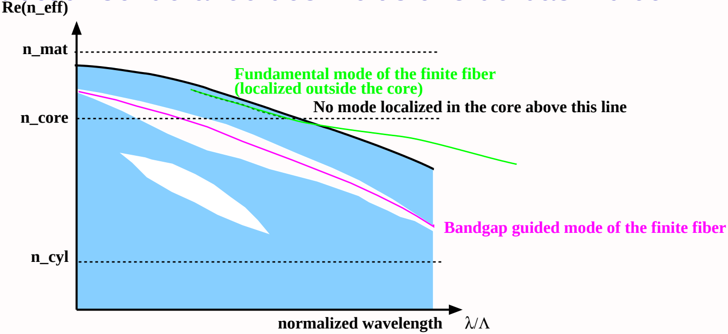

Figure: Schematic band diagram of a periodic array of inclusions of low refractive index n_{cyl} in a high refractive index matrix n_{mat} such that $n_{cyl} < n_{mat}$ together with the dispersion curve of the fundamental mode of the finite size MOF such that $n_{cyl} < n_{core} < n_{mat}$. In this case, the fundamental mode has a transition, it delocalizes from the low index core to the higher index region surrounding it when the wavelength decreases.

Interprétation en termes de diagramme de bandes

FOM à cœur plein avec des inclusions de haut indice (type ARROW)

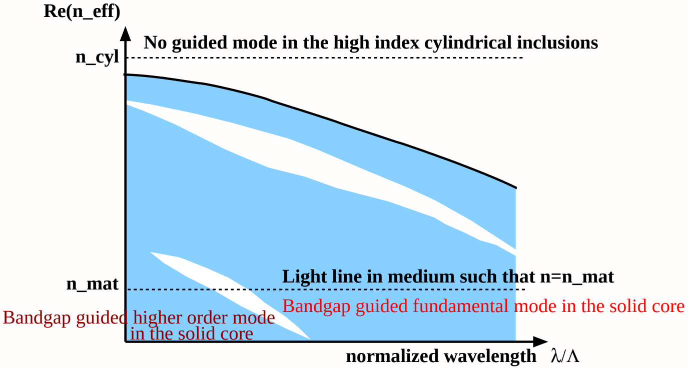

Figure: Schematic band diagram of a periodic array of inclusions of high refractive index n_{cyl} in a low refractive index matrix n_{mat} such that $n_{cyl} > n_{mat}$ together with the dispersion curves of the fundamental mode and a higher order mode of the finite size MOF such that $n_{core} = n_{mat}$.

Principales propriétés des FOM à cœur plein
Un diagramme de phase pour le mode fondamental

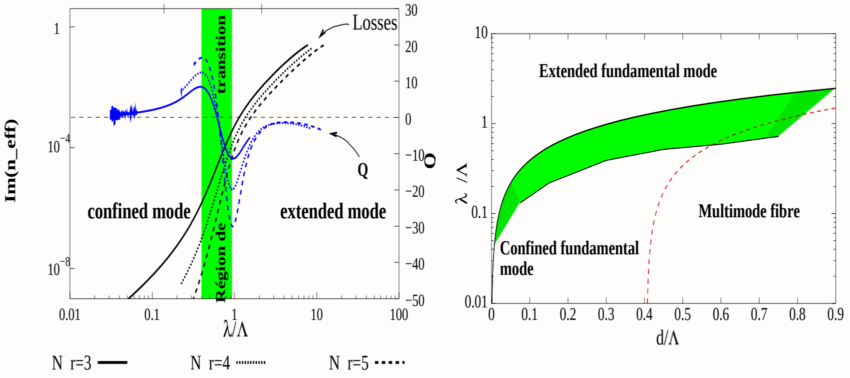

Comparaison des dispersions chromatiques du guide en fonction de l'indice de la matrice

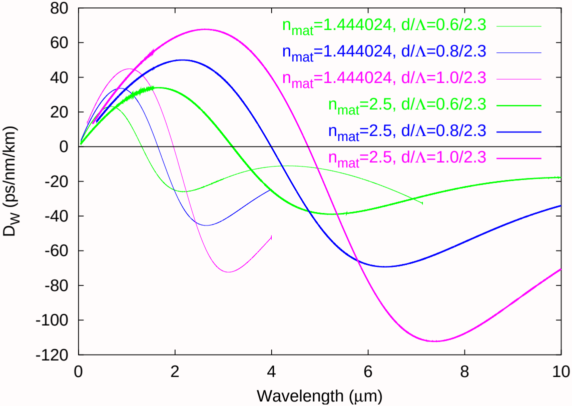

Figure: indices: n_{mat}=1.444024 (traits fins) et n_{mat}=2.5 (traits épais) pour plusieurs valeurs du rapport d/Λ pour des structures avec $N_r = 3$.